OPEN ACCESS
IOP PUBLISHING
SCIENCE AND TECHNOLOGY OF ADVANCED MATERIALS
Sci. Technol. Adv. Mater. **14** (2013) 055002 (10pp)
doi:10.1088/1468-6996/14/5/055002

Correlation between properties and microstructure of laser sintered porous β-tricalcium phosphate bone scaffolds

Cijun Shuai[1,2], Pei Feng[1], Liyang Zhang[3], Chengde Gao[1], Huanlong Hu[1], Shuping Peng[3,4] and Anjie Min[5]

[1] State Key Laboratory of High Performance Complex Manufacturing, Central South University, Changsha 410083, People's Republic of China
[2] Department of Regenerative Medicine & Cell Biology, Medical University of South Carolina, Charleston, SC 29425, USA
[3] Cancer Research Institute, Central South University, Changsha 410078, People's Republic of China
[4] Department of Obstetrics, Gynecology and Reproductive Sciences, Yale University School of Medicine, New Haven, CT, USA
[5] Department of Oral and Maxillofacial Surgery, Xiangya Hospital, Central South University, Changsha 410078, People's Republic of China

E-mail: shuping@csu.edu.cn (Shuping Peng) and william0732@csu.edu.cn (Anjie Min)

Received 6 April 2013
Accepted for publication 24 June 2013
Published 10 September 2013
Online at stacks.iop.org/STAM/14/055002

Abstract
A porous β-tricalcium phosphate (β-TCP) bioceramic scaffold was successfully prepared with our homemade selective laser sintering system. Microstructure observation by a scanning electron microscope showed that the grains grew from 0.21 to 1.32 μm with the decrease of laser scanning speed from 250 to 50 mm min^{-1}. The mechanical properties increased mainly due to the improved apparent density when the laser scanning speed decreased to 150 mm min^{-1}. When the scanning speed was further decreased, the grain size became larger and the mechanical properties severely decreased. The highest Vickers hardness and fracture toughness of the scaffold were 3.59 GPa and 1.16 MPa m$^{1/2}$, respectively, when laser power was 11 W, spot size was 1 mm in diameter, layer thickness was 0.1–0.2 mm and laser scanning speed was 150 mm min^{-1}. The biocompatibility of these scaffolds was assessed *in vitro* with MG63 osteoblast-like cells and human bone marrow mesenchymal stem cells. The results showed that all the prepared scaffolds are suitable for cell attachment and differentiation. Moreover, the smaller the grain size, the better the cell biocompatibility. The porous scaffold with a grain size of 0.71 μm was immersed in a simulated body fluid for different days to assess the bioactivity. The surface of the scaffold was covered by a bone-like apatite layer, which indicated that the β-TCP scaffold possesses good bioactivity. These discoveries demonstrated the evolution rule between grain microstructure and the properties that give a useful reference for the fabrication of β-TCP bone scaffolds.

Keywords: SLS, β-TCP, laser scanning speed, grain size, mechanical and biological properties

1. Introduction

Bioceramics, including β-tricalcium phosphate [β-TCP, $Ca_3(PO_4)_2$], hydroxyapatite [HAP, $Ca_{10}(PO_4)_6(OH)_2$] and so on, have been considered as the most promising materials

for bone scaffolds due to their excellent biocompatibility, bioactivity and bioresorbability characteristics [1]. However, the dissolution rate and osteoconduction of HAP are too slow, although it has good bioactivity [2, 3]. β-TCP has been used for the fabrication of scaffolds due to its good degradation rate and bone formation ability [4–6]. The β-TCP scaffold degrades gradually and was replaced by new living bone after some time [7]. Moreover, the degradation of β-TCP can offer abundant calcium and phosphorus elements to the osteoblasts, and promote the formation of new bone [8]. Although some work has already been done with β-TCP, the mechanical strength and fracture toughness of β-TCP ceramics are still poor, which restricts its use to low load-bearing applications [9]. It is generally believed that only when the conditions of high density and fine grains are simultaneously met, the mechanical properties of bioceramics are guaranteed [10, 11]. Studies showed a proportionality relationship between the density and fracture toughness of calcium phosphate bioceramics [12]. The smaller the grain size of bioceramics, the higher the fracture toughness, as well as the compressive strength and tensile strength [13].

Conventional sintering usually requires temperatures above 1000 °C and takes hours or even dozens of hours in order to achieve densification. The high sintering temperature and long sintering time cause larger grain size, which are detrimental to the mechanical properties [14]. Hence, conventional sintering cannot meet the requirement of both dense and very fine grain size at the same time [15]. However, a laser can reduce the sintering time to a few seconds, or even milliseconds, because of its high energy density, which can achieve sintering densification and restrict grain growth due to the rapid sintering and rapid cooling. Mondal *et al* [16] reported that microwave sintering could be used to fabricate consolidated tungsten-based alloys with finer grain size at higher temperature with an overall reduction of sintering time by up to 80% compared with the conventional sintering method. Chaim *et al* [17] found that the spark plasma sintering (SPS) was very attractive for densification and preservation of the nanocrystalline character in ceramics at a temperature of 1375 °C for 3 min. Although these methods can sinter ceramics to near full densification with finer grain size, these methods are difficult to realize the three-dimensional interconnected porous structure, which is a favorable environment for the scaffold to allow cell attachment, proliferation and differentiation, and to provide pathways for biofluids [18].

A laser can be used to prepare the porous structure through the selective manufacturing process. It can achieve accurate control of the pore size, as well as the complex contour and internal structure of bone scaffolds [19, 20]. Several papers have reported the use of this method for the preparation of porous scaffolds [21–25]. Duan *et al* [21] used calcium phosphate (Ca–P)/poly(hydroxybutyrate-co-hydroxyvalerate) and carbonated hydroxyapatite/poly(L-lactic acid) nanocomposite microspheres to fabricate three-dimensional nanocomposite scaffolds. Dyson *et al* [22] used apatite–wollastonite (A–W) composites as raw material to produce porous glass-ceramic scaffolds. Lohfeld *et al* [23] used polycaprolactone (PCL) and PCL/TCP mixtures with up to 50 wt% TCP to fabricate bone tissue engineering scaffolds. They mainly used polymer or glass as the matrix and ceramics as the enhancement phase to prepare scaffolds. However, the natural/synthetic polymers used as scaffold material very easily cause an inflammation response and have a low capacity for facilitation of cellular responses [26, 27].

Table 1. Process parameters of sintering experiment.

Item	Condition
Laser power (W)	11
Spot diameter (mm)	1.0
Powder layer thickness (mm)	0.1–0.2
Sintering speed (mm · min^{-1})	50 100 150 200 250

In the paper, pure β-TCP powders were used as raw materials, and the porous bioceramic scaffolds with controllable porous structure were prepared with our homemade selective laser sintering (SLS) system. The effects of microstructure on the properties of the scaffolds were investigated when the pure β-TCP powders were sintered at different laser scanning speeds. The surface and cross-sectional morphology, microstructure, and cell morphology of the scaffolds were observed. The phase and chemical composition of the initial β-TCP powder were also characterized. The mechanical properties of porous scaffolds were assessed in terms of Vickers hardness and fracture toughness. An *in vitro* biocompatibility test was carried out using hBMSCs and MG63 cells. In addition, the *in vitro* bioactivity of the obtained porous scaffolds was evaluated by soaking in simulated body fluid (SBF) for various periods of time.

2. Materials and methods

2.1. Preparation of porous β-TCP scaffolds with SLS

The β-TCP powder (Ca/P ratio: 1.5 ± 0.03; purity: $\geqslant 98\%$; particle size: 0.1–0.3 μm) used in this study was purchased from Kunshan Chinese Technology New Materials Co. Ltd. The sintering experiments of β-TCP powder were carried out on the homemade SLS system [28, 29]. Core features of this SLS system include the optical focusing system, the control system and the three-dimensional motion platform. The laser sintering machine is loaded with a 100 W CO_2 laser (model Firestar® t-Series, Synrad Co., USA). The optical devices (Haas Co., USA) are used in the optical focusing system to focus the incident optical beam into a spot with a small size. The minimum spot diameter can reach 50 μm. The three-dimensional motion platform and the laser sinter parameters are controlled by a 6050 motion control card (Dong Fang Jia Hong Co.).

The sintering was performed by varying the laser scanning speed while the other parameters were kept the same (table 1). Numerical simulation of the dynamic temperature field during the SLS of calcium phosphate bioceramics powder has been published in our previous paper [30]. The sintering process and a sintered layer are shown in figures 1(a) and (b), respectively. Scaffolds were fabricated

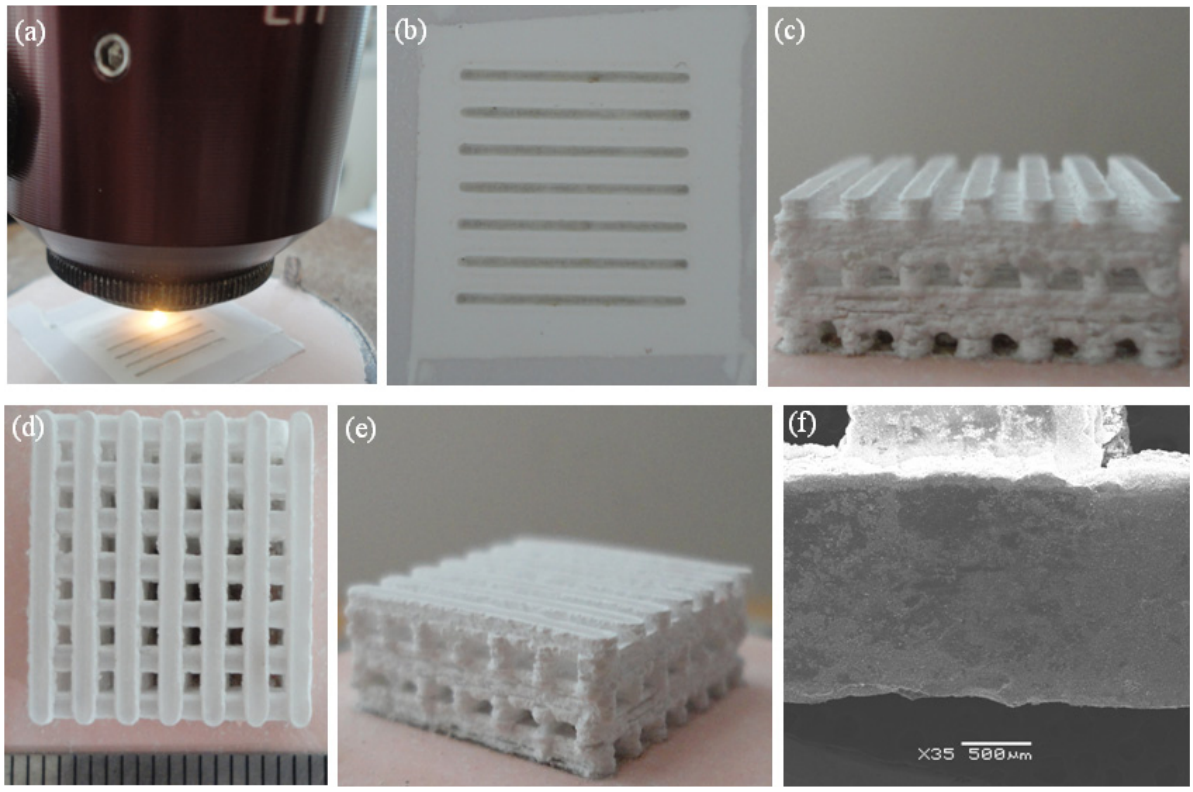

Figure 1. (a) The laser selectively sinters the β-TCP powder along the predetermined path. (b) A sintered layer. (c)–(e) Macro morphology of porous β-TCP bioceramic scaffolds. The scaffold is about 18 mm × 18 mm × 5 mm ($W \times L \times H$) in size and has a porosity of 46.2%. The pores are about 1.4 mm × 1.4 mm ($W \times L$). Three-dimensional structures exhibit tailored porosity, pore size and interconnectivity. (f) Microstructure of a single sintered path; the width of the solid pillar is about 1.4 mm.

layer by layer with the powder layer thickness of 0.1–0.2 mm. The excess powder surrounding the scaffolds was brushed off and unsintered powder was removed from the scaffold interstices by repeatedly rinsing with deionized water after SLS processing was completed. The surface of the laser sintered β-TCP porous scaffold looks smooth without cracks and previous designed macropores can be seen clearly (figures 1(c)–(e)).

The porosity of the porous scaffold was calculated by [31]

$$\text{Porosity} = \frac{V_m - V_p}{V_m} \times 100\%, \tag{1}$$

where V_m is the total volume of the porous scaffold (mm^3), which was calculated based on the geometry of the porous scaffold ($W \times L \times H$). V_p is the actual volume (mm^3), which was measured using the Archimedes principle [32]. The scaffold is about 18 mm × 18 mm × 5 mm ($W \times L \times H$), so the total volume of the porous scaffold was 1620 mm^3. The actual volume was measured in water, which was 871.56 mm^3. According to equation (1), the porosity of the porous β-TCP scaffolds was calculated as 46.2%. The pores are about 1.4 mm × 1.4 mm ($W \times L$). The scaffold is highly porous, and three-dimensional structures exhibit tailored porosity, pore size and interconnectivity. The microstructure of a single sintered path is shown in figure 1(f). It can be seen that the width of the solid pillar is about 1.4 mm.

2.2. Characterization techniques

The phases present were identified by an x-ray diffractometer (XRD, D8-ADVANCE, German) with a Cu Kα radiation source operating at 40 kV and 40 mA. Fourier transform infrared (FTIR) spectra of the starting powder were obtained by using a Nicolet^{TM} 6700 spectrometer (Thermo Scientific, USA). Prior to FTIR analyses, the powder was mixed with KBr and pressed into pellets. Porous β-TCP bioceramic scaffolds fabricated at various laser scanning speeds were examined using a scanning electron microscope (SEM, FEI Quanta-200, USA). Gold was primarily coated on the scaffold surface for 30 s to reduce the charging effect during the measurements. Microstructural evolution and grain size were also examined after the scaffolds were etched with 5% hydrofluoric acid (HF) for 2 min to delineate the grain boundaries.

Hardness and fracture toughness. Indentation of the scaffolds was obtained and measured with a Vickers microindenter (HXD-1000TM/LCD, Digital Micro Hardness Tester, Shanghai Taiming Optical Instrument Co. Ltd) at a load of 300 gf (2.942 N) applied for 10 s. Prior to indentation, the scaffold samples were inlaid in epoxy vertically with an inlaying machine (XQ-2B, $\Phi 22^{*}15$). The hardness of scaffolds was calculated according to equation (2) [33]. The fracture toughness was calculated using equation (3), which was derived from the model proposed by Evans and Charles [34]. The average hardness and fracture toughness

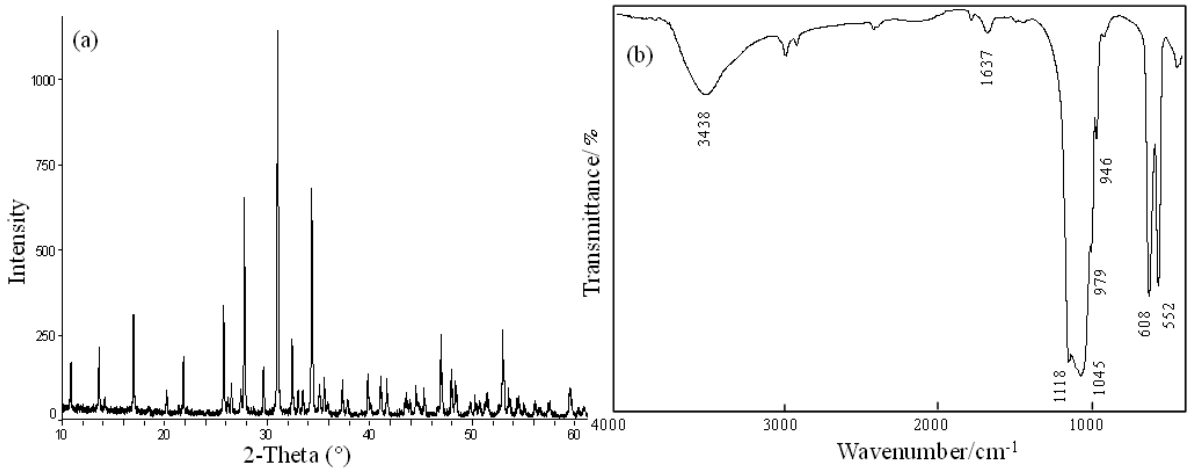

Figure 2. XRD pattern (a) and FTIR spectra (b) of the starting β-TCP powder.

values of six indents were calculated and the maximum error was less than 5%:

$$H_V = 0.1891F/d^2, \tag{2}$$

where F is the applied load, d is the mean length of the diagonal lines and H_V refers to the value of Vickers hardness.

$$K_{IC} = 0.0824(P/C^{1.5}), \tag{3}$$

where P is the applied indenter load and C the radial crack length measured from the center point of the indentation impression.

MG63 cells (American Type Culture Collection, Rockville, MD) were cultured in Dulbecco's modified Eagle's medium (DMEM, Gibco, Carlsbad, CA), containing 10% fetal bovine serum and 1% penicillin–streptomycin at 37 °C in 5% CO_2. The MG63 cell line was originally derived from a human osteosarcoma and has been shown to exhibit many characteristics of premature osteoblasts, making it an attractive model for *in vitro* studies. Human bone marrow mesenchymal stem cells (hBMSCs) were isolated from adult human bone marrow aspirates of ribs of patients undergoing thoracic surgery. The sample collection was informed and approved by the patients with signed informed consent forms and the ethical review committees of Second Xiangya Hospital. The cells were expanded in non-differentiating MSC growth medium supplemented with 10% fetal bovine serum, 1% penicillin–streptomycin and 2 mM glutamine, in a humidified atmosphere at 37 °C in 5% CO_2. The cells were cultured in cell culture dishes for 1 day prior to seeding. All prepared scaffolds were sterilized by immersion in 70% ethanol for 3 h, followed by immersion in phosphate buffered saline for 1 day. Cells at a density of 4×10^5 cells were added to each scaffold and allowed to attach to the matrix for 30 min before adding enough medium to submerge the scaffolds. Cell culture was allowed to continue for 14 days, changing the medium every 2 days in the static cultures. Adhesion assays were performed three times, each in triplicate. After 14 days of culture, scaffolds were fixed in 2.5% glutaraldehyde and rinsed three times with PBS. All the samples were then dried at room temperature, sputter coated with gold and observed with SEM (FEI Quanta-200, USA) for investigating cell adhesion and proliferation on the prepared scaffolds.

An *in vitro* bioactivity test was carried out by soaking the scaffolds in 2 ml of SBF (142.0 Na^+, 5.0 K^+, 1.5 Mg^{2+}, 2.5 Ca^{2+}, 147.8 Cl^-, 4.2 HCO_3^-, 1.0 HPO_4^{2-} and 0.5 SO_4^{2-}) in cell culture dishes and placing in an incubator at 37 °C for periods of 7, 14, 21 and 28 days. After soaking for different soaking periods, the scaffolds were taken out from SBF, rinsed with deionized water and dried at 65 °C in an oven for 2 days. The surface and cross-section morphology of scaffolds after soaking in SBF for different times was analyzed by SEM. The elemental composition analysis of the crystals was conducted by energy dispersive spectroscopy (EDS).

3. Results and analysis

3.1. Initial powder

The XRD pattern of initial β-TCP powder is shown in figure 2(a). All peaks in the pattern are coincident with the standard pattern of β-TCP (JCPDS 09-0169) [35], and no other diffraction peaks are observed, which suggests the high purity of initial β-TCP powder. Sharp diffraction peaks in figure 2(a) indicate that the β-TCP powder has good crystallinity.

The FTIR spectrum of initial β-TCP powder is shown in figure 2(b). The FTIR spectra are dominated by the internal PO_4^{3-} bands, which are surrounded by the frequency values of 552–608 and 979–1118 cm^{-1} [36]. Besides the main peak at 979 cm^{-1}, another frequency peak at 946 cm^{-1} has formed. The results of FTIR spectra reveal that no other impurity phases such as calcium carbonate or calcium oxide are present in the initial β-TCP powder, which is consistent with the XRD result.

3.2. Microstructure analysis

SEM micrographs of the initial β-TCP and sintered β-TCP scaffolds without etching are shown in figures 3(a)–(c), respectively. The initial β-TCP particles are irregular with average sizes of 0.1–0.3 μm and loosely stack together

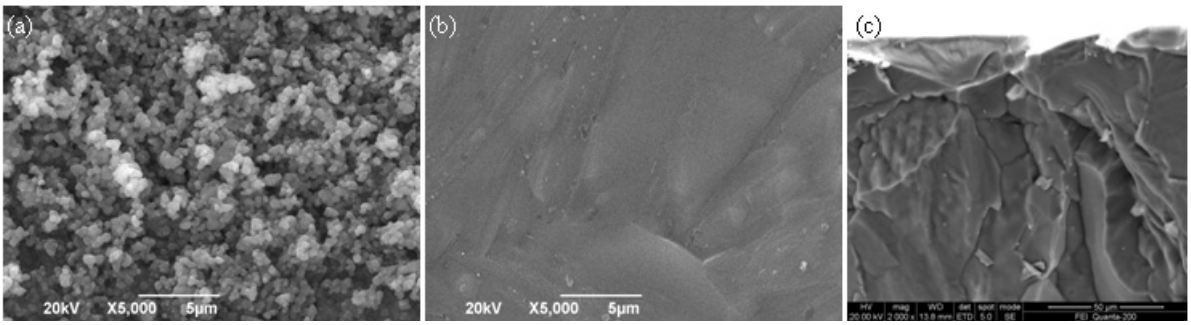

Figure 3. SEM micrographs acquired before etching: (a) the initial β-TCP powder; (b): the top view of the porous β-TCP scaffold; and (c) the cross-sectional view of the scaffold.

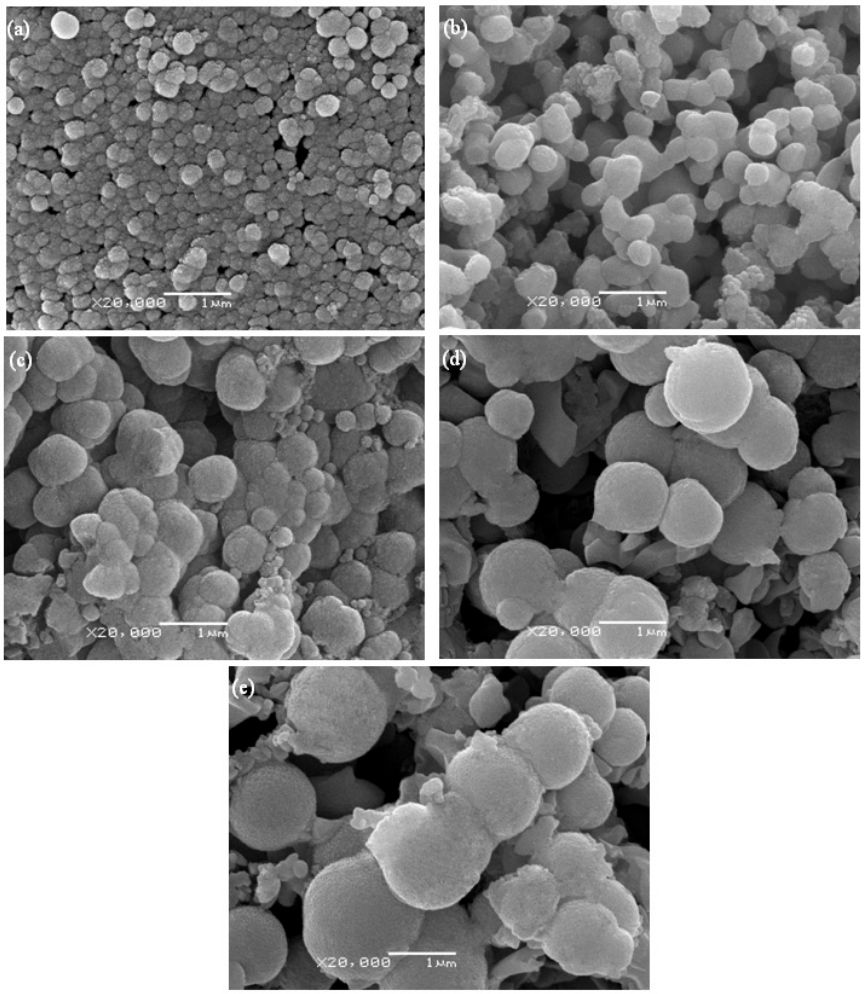

Figure 4. SEM micrographs after the sample was etched with 5% HF for 2 min: (a) $v = 250\,\text{mm}\,\text{min}^{-1}$; (b) $v = 200\,\text{mm}\,\text{min}^{-1}$; (c) $v = 150\,\text{mm}\,\text{min}^{-1}$; (d) $v = 100\,\text{mm}\,\text{min}^{-1}$; and (e) $v = 50\,\text{mm}\,\text{min}^{-1}$.

(figure 3(a)). The particles bond with each other and become a full block with smooth surface and high density after sintering (figure 3(b)). The cross-sectional view of the scaffold reveals an obvious lamellar structure without pores and microcracks (figure 3(c)). Sintering resulted in considerable densification of the scaffold, due to the removal of the micropores between the β-TCP particles in the solid pillars.

In order to further study the effect of laser scanning speeds on the microstructure and grain growth of the porous β-TCP scaffold, the scaffold's surface was etched to delineate the grain boundaries and observed under SEM in figure 4. The average grain sizes (G_a) were measured three times for each specimen using the linear intercept method from the SEM micrographs of etched surfaces. For grain size determination, five representative micrographs with a magnification of 5000× were analyzed. A series of random straight test lines were drawn through the micrograph. The total number of intersections of the line with grain boundaries was counted. The average grain sizes (G_a) were determined using the linear

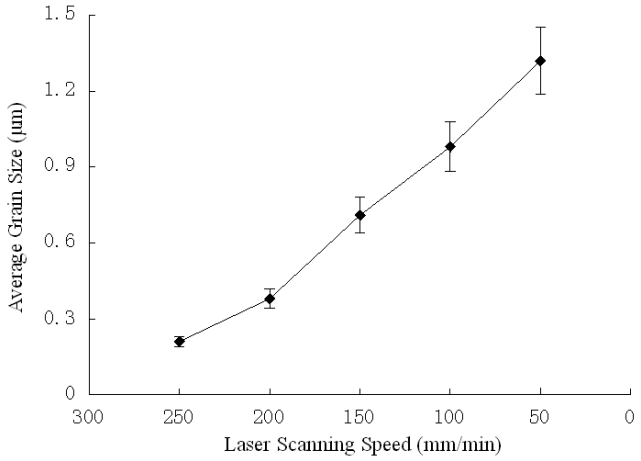

Figure 5. Trend of grain sizes in β-TCP sintered at various laser scanning speeds.

intercept technique following equation (4) [37]:

$$G_a = 1.5L/MN, \tag{4}$$

where 1.5 is the geometry-dependent proportionality constant, L is the total test line length, M is the magnification and N is the total number of intercepts.

The micrographs of etched surfaces show significant differences in microstructure under the various laser scanning speeds. It shows that the average grain size is 0.21 μm when the laser scanning speed is 250 mm min^{-1} (figure 4(a)). There are still many micropores of different sizes and shapes in the scaffold. The density is further improved with the reduction of the micropores when the laser scanning speed decreases to 200 mm min^{-1} (figure 4(b)). The grains grow to 0.38 μm in size under the driving force of grain boundary diffusion. The grains become peanut-like of 0.71 μm in size and bond with each other more closely when the laser scanning speed is 150 mm min^{-1} (figure 4(c)). And the density is significantly improved with the elimination of micropores. Little change is seen in density when the laser scanning speed decreases to 100 or 50 mm min^{-1} (figure 4(d) or (e)). However, the grain size becomes larger due to the high energy density and the average grain sizes of sintered β-TCP scaffolds become 0.98 or 1.32 μm, respectively. The trend of average grain size of sintered β-TCP under various laser scanning speeds is shown in figure 5. It can be observed that the average grain size increases on decreasing the laser scanning speed. The average grain size increases to 0.71 μm when the laser scanning speed decreases to 150 mm min^{-1}. The grain size becomes larger when the scanning speed is further decreased. Therefore, it could be concluded that the sintered β-TCP scaffold possesses both high density and fine grains with an optimum laser scanning speed of 150 mm min^{-1}.

3.3. Mechanical properties analysis

The bone scaffold is generally expected to possess suitable biomechanical properties so as to be compatible with natural bone. Studies show that scaffolds with high hardness values will also have good performance in wear resistance when implanted in bone defects [38]. Fracture toughness is an important parameter to assess the susceptibility of a scaffold to failure [39]. Thus, the average hardness and fracture toughness of sintered porous β-TCP scaffolds under different laser scanning speeds were measured six times for each specimen and shown in figure 6. It can be observed that the hardness and fracture toughness of the porous scaffold increased and then decreased as the laser scanning speeds decreased.

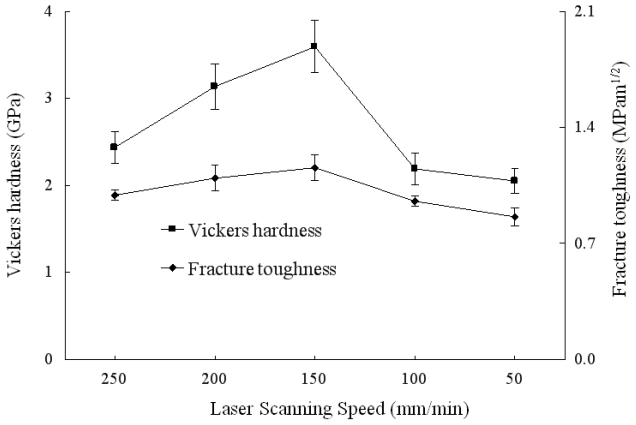

Figure 6. Vickers hardness and fracture toughness of β-TCP scaffolds as a function of laser scanning speeds.

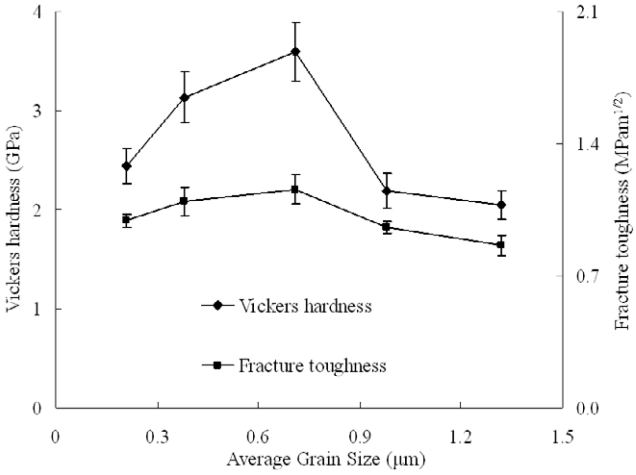

Figure 7. Vickers hardness and fracture toughness of β-TCP scaffolds as a function of average grain size.

The hardness and fracture toughness increase gradually mainly because of increasing of the density when the laser scanning speed decreases from 250 to 150 mm min^{-1} (figure 6). The larger grain size is the main reason that causes the decrease of hardness and fracture toughness of the scaffolds when the laser scanning speed decreases from 150 to 50 mm min^{-1}. Based on previous studies [40], the mechanical properties of the ceramics increase as the density increases and grain size decreases. Therefore, the laser scanning speed of 150 mm min^{-1} is considered to be optimum concerning the mechanical property of sintered β-TCP scaffolds.

The relationship between the mechanical properties (Vickers hardness and fracture toughness) and average grain size of β-TCP scaffolds is shown in figure 7. Vickers hardness gradually increases with the growth of β-TCP grains from 0.21 to 0.71 μm. The grains bond with each other closely and the β-TCP scaffold with the highest hardness is obtained when the average grain size is 0.71 μm. The hardness begins to decrease sharply when the average grain size is >0.71 μm. This will lead to poor mechanical properties of porous β-TCP bioceramic scaffolds when the average grain size is too large. The observed trends were the same for the fracture toughness and Vickers hardness. However, the mechanical properties of porous ceramic scaffolds depended not only on the grain size and density, but also on the porosity and percolation structure. When other conditions remain unchanged, the mechanical properties (compressive strength, bending strength and so on) of porous ceramic scaffolds decrease with the increase of porosity. The porosity of all the porous β-TCP was calculated as 46.2% under different laser scanning speeds (50–250 mm min^{-1}). When the porosity of all scaffolds remained the same, we compared the grain size and density for measuring the relationship between grain size or density and hardness and toughness.

It is known that the hardness and fracture toughness of ceramics are affected by a combination of the density and grain size [41]. The mechanical properties are mainly governed by the density when the grain size is below 0.71 μm. However, there is no obvious change in the density when the grain size is bigger than 0.71 μm. The hardness and fracture toughness are mainly determined by the average grain size. The grain size becomes larger when the laser scanning speed is slower (below 150 mm min^{-1}), which will cause the sharp decrease of hardness and fracture toughness.

It can be concluded from the above results and analysis that the porous β-TCP bioceramic scaffolds possess low density and thus poor mechanical properties when the laser scanning speed is too fast. A sharp decrease in the hardness and fracture toughness appears due to the larger grain size when the laser scanning speed decreases to below 150 mm min^{-1}. Therefore, the optimum processing parameters in this sintering experiment are obtained and shown as follows: the laser scanning speed is 150 mm min^{-1}, the laser power is 11 W and the spot diameter is 1.0 mm. The porous β-TCP bioceramic scaffolds have an average grain size of 0.71 μm, and the highest hardness and fracture toughness values are 3.59 GPa and 1.16 MPa m$^{1/2}$, respectively. Raynaud *et al* [42] measured a fracture toughness of 1.0 ± 0.1 MPa m$^{1/2}$ in hot pressed HAP/TCP ceramics with an average 200 nm grain size. The highest hardness is higher than the H_V value of 2.64 ± 0.35 GPa for β-TCP ceramics reported by Lin *et al* [43]. The highest fracture toughness is slightly above the K_{IC} value of 0.92 ± 0.04 MPa m$^{1/2}$ for β-TCP ceramics reported by Chen *et al* [44]. The high fracture toughness is closer to that of human cortical bone [45], which can improve the mechanical compatibility of scaffolds.

3.4. In vitro *cell culture*

Cell attachments and proliferation assays were analyzed to investigate the effect of the grain size of β-TCP scaffolds on osteoblasts and to evaluate the biological performance of porous scaffolds. The morphology of the human osteosarcoma MG63 cells and hBMSCs cultured onto the β-TCP scaffolds is shown in figures 8 and 9. MG63 cells and hBMSCs were observed to attach to all the prepared scaffolds, which indicate that all the prepared scaffolds were non-toxic to the cells. A few MG63 cells and hBMSCs were observed on the scaffold surface and did not spread well when the grain size was 1.32 μm (figures 8(a) and 9(a)). The number of cells attached on the β-TCP scaffold increased with the decreasing of grain size from 1.32 to 0.21 μm. Cells dramatically proliferated and aggregated with each other to form stratified cell layers on the surface when the grain size was 0.21 μm (figures 8(e) and 9(c)). These results show that the small grain size is more favorable for cell attachment than the large grain size. These results are in good agreement with those reported [46, 47] in the literature on the effect of grain size on the ability to support cell adhesion and proliferation. Kim *et al* [46] studied the mouse fibroblast cell line 3T3 response to ultrafine grained titanium and revealed that the smaller grain size on the Ti specimen surface results in higher surface energy, which is more favorable for cell adherence. He *et al* [47] investigated the effect of surface microstructure on the serum protein adsorption and the biological performance of osteoblasts cultured *in vitro*, when seeded onto the surface of ceramics with different grain sizes. It was found that the number of adherent cells on nano-sized HAP was significantly greater than that on the conventional HAP and micron-sized HAP.

3.5. In vitro *bioactivity*

The surface and cross-sectional morphology and EDS spectra of the scaffold with a grain size of 0.71 μm after immersion in the SBF solution for 7, 14, 21 and 28 d are depicted in figure 10. It can be seen that granular crystals appeared on the surface of the scaffold soaked in SBF for 7 d (figure 10(a)). After 14 d of immersion, the surface of the scaffold was covered by a layer of worm-like crystals (figure 10(d)). After 21 d, the deposited layer became denser and the crystal layer consisted of numerous flake-like crystals (figure 10(g)). The 28 d of immersion resulted in a thick and dense layer with a sponge-like morphology (figure 10(j)). The cross-sectional views of the scaffold after immersion in the SBF solution for 7, 14, 21 and 28 d are shown in figures 10(b), (e), (h) and (k). A continuous layer with irregular thickness was formed on the surface of the scaffold after immersion in SBF. The thickness of the crystal layer increased obviously with the increase in soaking time. The crystal layer grows uniformly along the cross-section of the scaffold after 28 d of immersion (figure 10(k)). The EDS spectra of the crystal layer on the scaffold surface indicated that the crystals were mainly composed of Ca, P, O and C elements (figures 10(c), (f), (i) and (l)). The EDS results indicated the presence of Ca

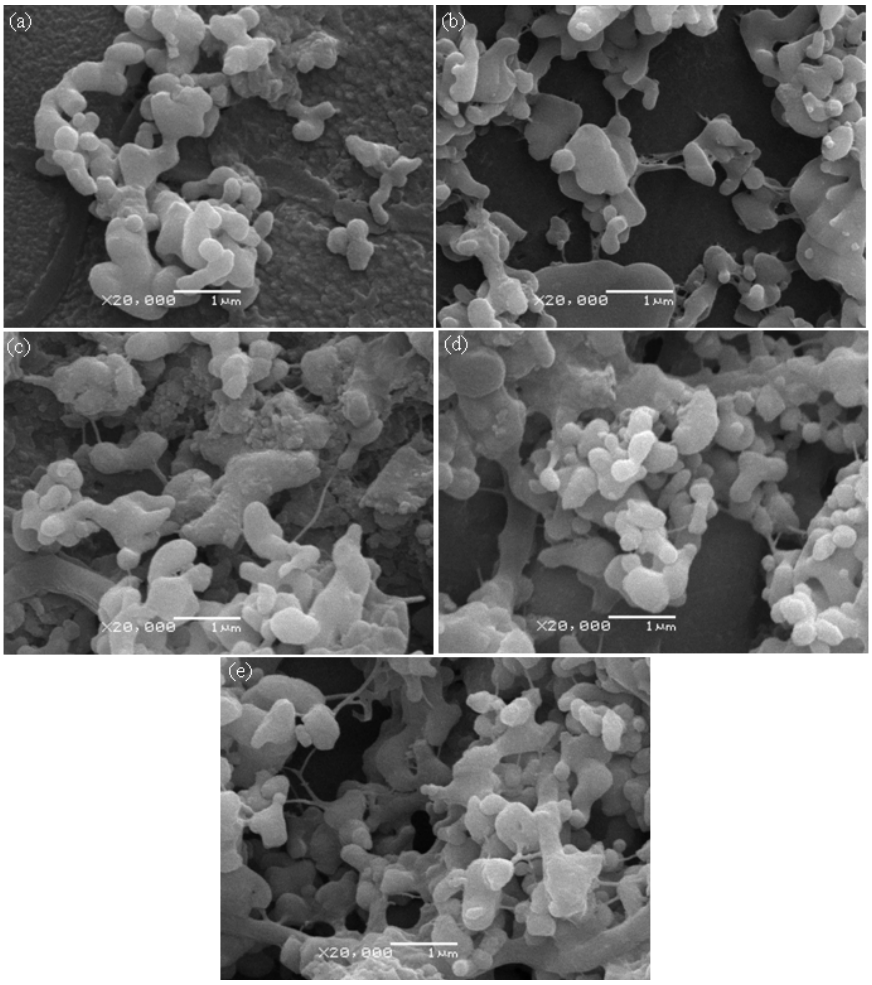

Figure 8. SEM morphology of MG63 cells cultured onto β-TCP scaffolds with grain sizes of (a) 1.32 μm, (b) 0.98 μm, (c) 0.71 μm, (d) 0.38 μm and (e) 0.21 μm.

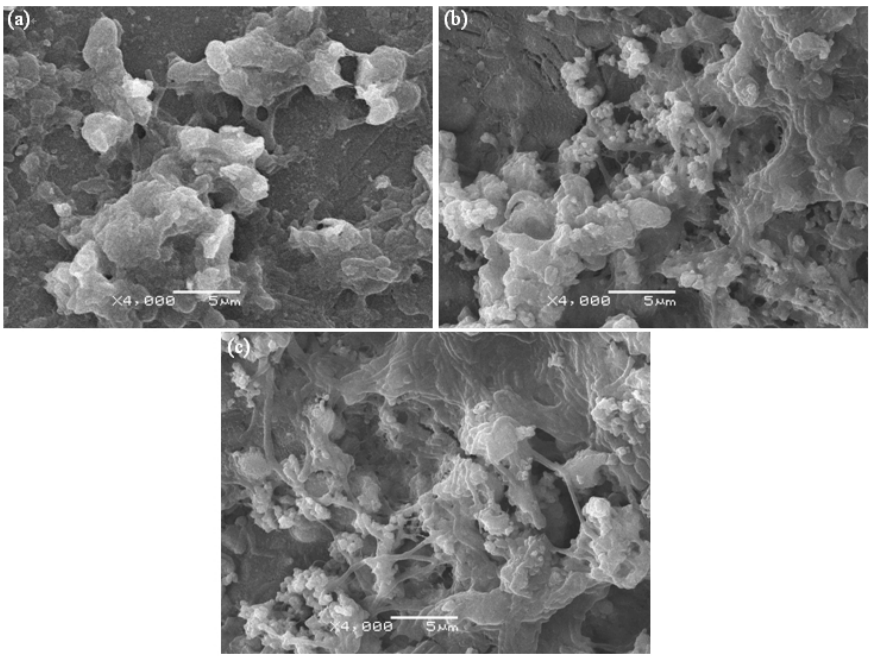

Figure 9. SEM morphology of hBMSCs cultured onto β-TCP scaffolds. (a) 1.32 μm, (b) 0.71 μm and (c) 0.21 μm.

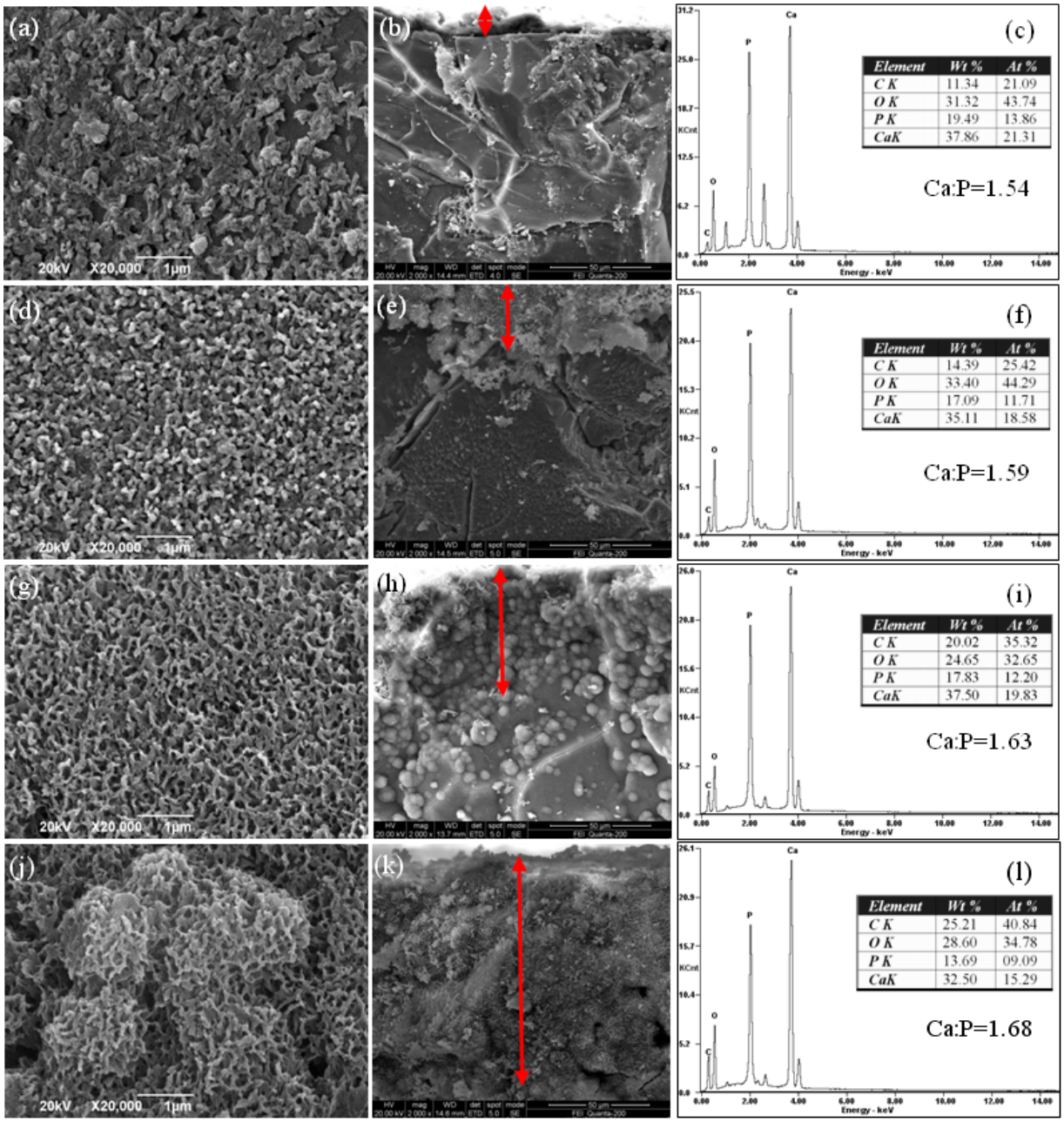

Figure 10. SEM images (surface and cross-sectional) and EDS traces of the β-TCP porous scaffold with a grain size of 0.71 μm after SBF incubation for different times: (a)–(c) for 7 d, (d)–(f) for 14 d, (g)–(i) for 21 d and (j)–(l) for 28 d.

and P consistent with the typical deposition of a bone-like apatite layer. The element C in the scaffold was attributed to the dissolution of CO_2 in air [48]. The CO_3^{2-} might substitute the PO_4^{3-} in apatite, which was similar to the composition of biological apatite from natural bone mineral [49]. It clearly showed that the C contents increased from 11.34 to 25.21 wt% on increasing the SBF immersion time. The Ca/P ratio of the apatite layer was 1.54 after 14 d of immersion. On further increasing the time to 28 d, the Ca/P ratio increased to 1.68, which was similar to the ratio of HAP. The Ca/P ratio tendency to increase with immersion time was in agreement with the literature reported by Oliveira *et al* [50]. It is possible to form a bone-like apatite layer on the scaffold surface when the Ca and P ions react with other ions in the SBF solution. The formation of a bone-like apatite layer on biomaterials is assumed to be the precondition for their osteoconductivity to induce bone formation [51]. This rough surface layer encourages bone ingrowth and provides mechanical fixation of the implant to the surrounding bone. The apatite layer could produce an acceleration in bone growth, improving the short-term implant response [52]. The surface of the scaffold was covered by an apatite layer, which indicated that the β-TCP scaffold possesses good osteoinductivity.

4. Conclusions

A β-TCP scaffold with porous structure was obtained with a homemade SLS system. The effects of microstructure on the

properties of β-TCP scaffolds were studied under different laser scanning speeds. The results show that the scaffold's mechanical properties and cell compatibility are directly related to its microstructure. The apatite layer formed on the surface of the scaffold soaked in SBF, which indicated that the β-TCP scaffold possesses good osteoinductivity. The apatite layer gradually became thick with an increase in the immersion time. An optimum porous scaffold with the highest mechanical properties and fine grain size can be eventually obtained when the laser scanning speed is $150\,\mathrm{mm\,min^{-1}}$. The matching criteria were established between the properties and microstructure parameters. It provides guidance for optimizing the fabrication technology to prepare porous β-TCP bioceramic scaffolds with further high performance.

Acknowledgments

This work was supported by the following funds: (i) the Natural Science Foundation of China (51222506, 81000972, 81102045); (ii) the foundation for the author of national excellent doctoral dissertation of PR China (201032); (iii) Program for New Century Excellent Talents in University (NCET-10-0792, NCET-12-0544); (iv) The Fundamental Research Funds for the Central Universities (2011JQ005); (v) project supported by the Fok Ying-Tong Education Foundation, China (131050); (vi) Open Research Fund of State Key Laboratory of Transient Optics and Photonics, Chinese Academy of Sciences; and (vii) The Open-End Fund for the Valuable and Precision Instruments of Central South University.

References

[1] Vivanco J, Slane J, Nay R, Simpson A and Ploeg H L 2011 *J. Mech. Behav. Biomed.* **4** 2150
[2] Li S, Izui H, Okano M and Watanabe T 2008 *J. Biomech. Sci. Eng.* **3** 1
[3] Macchetta A, Turner I G and Bowen C R 2009 *Acta Biomater.* **5** 1319
[4] Santos C F L, Silva A P, Lopes L, Pires I and Correia I J 2012 *Mater. Sci. Eng.* C **32** 1293
[5] Perera F H, Martínez-Vázquez F J, Miranda P, Ortiz A L and Pajares A 2010 *Ceram. Int.* **36** 1929
[6] Sharaf B, Faris C B, Abukawa H, Susarla S M, Vacanti J P, Kaban L B and Troulis M J 2012 *J. Oral Maxillofac. Surg.* **70** 647
[7] Manjubala I, Sivakumar M, Sureshkumar R V and Sastry T P 2002 *J. Biomed. Mater. Res.* **63** 200
[8] He S Y, Sun Y, Chen M F, Liu D B and Ye X Y 2011 *Trans. Nonferrous. Met. Soc. China* **21** 814
[9] Frantzén J *et al* 2011 *Int. J. Biomater.* **2011** 109638
[10] He Z M, Ma J and Wang C 2005 *Biomaterials* **26** 1613
[11] O'Flynn K P, Twomey B, Breen A, Dowling D P and Stanton K T 2011 *J. Mater. Sci., Mater. Med.* **22** 1625
[12] Dorozhkin S V 2010 *J. Funct. Biomater.* **1** 22
[13] Ghosh S K, Prakash A, Datta S, Roy S K and Basu D 2010 *Bull. Mater. Sci.* **33** 7
[14] Yihan L, Ming Z and Jing L 2012 *Light Metals 2012* (New York: Wiley) p 1389
[15] Teresa H, Jean G and Alicia C 2009 *Adv. Eng. Mater.* **11** 615
[16] Mondal A, Upadhyaya A and Agrawal D 2006 *PMRM Workshop (Heavy Alloy Penetrator Project, Tiruchirappalli)*
[17] Chaim R, Kalina M and Shen J Z 2007 *J. Eur. Ceram. Soc.* **27** 3331
[18] Ramay H R and Zhang M 2003 *Biomaterials* **24** 3293
[19] Gittard S D and Narayan R J 2010 *Expert Rev. Med. Devices* **7** 343
[20] Hutmacher D W 2001 *J. Biomater. Sci. Polym. Edn* **12** 107
[21] Duan B, Wang M, Zhou W Y, Cheung W L, Li Z Y and Lu W W 2010 *Acta Biomater.* **6** 4495
[22] Dyson J A, Genever P G, Dalgarno K W and Wood D J 2007 *Tissue Eng.* **13** 2891
[23] Lohfeld S, Cahill S, Barron V, McHugh P, Dürselen L, Kreja L, Bausewein C and Ignatius A 2012 *Acta Biomater.* **8** 3446
[24] Duan B, Cheung W L and Wang M 2011 *Biofabrication* **3** 015001
[25] Simpson R L, Wiria F E, Amis A A, Chua C K, Leong K F, Hansen U N, Chandrasekaran M and Lee M W 2008 *J. Biomed. Mater. Res.* B **84** 17
[26] Seeherman H and Wozney J M 2005 *Cytokine Growth Factor Rev.* **16** 329
[27] Griffith C K, Miller C, Sainson R C, Calvert J W, Jcon N L, Hughes C C and George S C 2005 *Tissue Eng.* **11** 257
[28] Shuai C, Gao C, Nie Y, Hu H, Zhou Y and Peng S 2011 *Nanotechnology* **22** 1
[29] Shuai C, Gao C, Nie Y, Hu H, Qiu H and Peng S 2010 *J. Biomed. Nanotechnol.* **6** 370
[30] Shuai C, Feng P, Gao C, Nie Y, Zhou Y and Peng S 2013 *Math. Comput. Model. Dyn.* **19** 1
[31] Hsieh W C, Chang C P and Lin S M 2007 *Colloids Surf.* B **57** 250
[32] Macione J, DePaula C A, Guzelsu N and Kotha S P 2010 *J. Mech. Behav. Biomed.* **3** 405
[33] Siggelkow L, Burkhardt U, Kreiner G, Palm M and Stein F 2008 *Mater. Sci. Eng.* A **497** 174
[34] Evans A G and Charles E A 1976 *J. Am. Ceram. Soc.* **59** 371
[35] Cacciotti I, Bianco A, Lombardi M and Montanaro L 2009 *J. Eur. Ceram. Soc.* **29** 2969
[36] Zenobi M C, Luengo C V, Avena M J and Rueda E H 2008 *Spectrochim. Acta* A **70** 270
[37] Wurst J C and Nelson J A 1972 *J. Am. Ceram. Soc.* **55** 109
[38] Heness G and Nissan B B 2004 *Mater. Forum* **27** 104
[39] Ramay H R R and Zhang M 2004 *Biomaterials* **25** 5171
[40] Rice W R 1993 *J. Mater. Sci.* **28** 2187
[41] Evis Z and Arcaklioglu E 2011 *Ceram. Int.* **37** 1147
[42] Raynaud S, Champion E, Lafon J P and Assollant D B 2002 *Biomaterials* **23** 1081
[43] Lin K, Chang J, Lu J, Wu W and Zeng Y 2007 *Ceram. Int.* **33** 979
[44] Chen B Q, Zhang Z Q, Zhang J X, Lin Q L and Jiang D L 2008 *Mater. Sci. Eng.* C **28** 1052
[45] Ramesh S, Tan C Y, Sopyan I, Hamdi M and Teng W D 2007 *Sci. Technol. Adv. Mater.* **8** 124
[46] Kim T N, Balakrishnan A, Lee B C, Kim W S, Dvorankova B, Smetana K, Park J K and Panigrahi B B 2008 *J. Mater. Sci. Mater. Med.* **19** 553
[47] He H W, Li G D, Li B and Chen Z Q 2008 *Appl. Surf. Sci.* **255** 565
[48] Wen C, Guan S, Peng L, Ren C, Wang X and Hu Z 2009 *Appl. Surf. Sci.* **255** 6433
[49] Evans G P, Bemire J C, Currey J D and Bonfield W 1990 *J. Mater. Sci. Mater. Med.* **1** 38
[50] Oliveira A L, Alves C M and Reis Rl 2002 *J. Mater. Sci. Mater. Med.* **13** 1181
[51] De Aza A H, Velásquez P, Alemany M I, Pena P and De Aza P N 2007 *J. Am. Ceram. Soc.* **90** 1200
[52] Aparicio C, Rodriguez D and Gil F J 2011 *Mater. Sci. Eng.* C **31** 320